Self-powered p-NiO/n-ZnO heterojunction ultraviolet photodetectors fabricated on plastic substrates

Md Rezaul Hasan, Ting Xie, Sara C. Barron, Guannan Liu, Nhan V. Nguyen, Abhishek Motayed, Mulpuri V. Rao, and Ratan Debnath

Citation: APL Materials **3**, 106101 (2015); doi: 10.1063/1.4932194
View online: http://dx.doi.org/10.1063/1.4932194
View Table of Contents: http://aip.scitation.org/toc/apm/3/10
Published by the American Institute of Physics

Articles you may be interested in

Self-powered narrowband p-NiO/n-ZnO nanowire ultraviolet photodetector with interface modification of Al_2O_3
Applied Physics Letters **110**, 123504 (2017); 10.1063/1.4978765

Ultraviolet electroluminescence from ZnO/NiO-based heterojunction light-emitting diodes
Applied Physics Letters **95**, 013509 (2009); 10.1063/1.3176440

High-performing visible-blind photodetectors based on SnO_2/CuO nanoheterojunctions
Applied Physics Letters **107**, 241108 (2015); 10.1063/1.4938129

Fabrication and photoresponse of a pn-heterojunction diode composed of transparent oxide semiconductors, p–NiO and n–ZnO
Applied Physics Letters **83**, 1029 (2003); 10.1063/1.1598624

High-performance zero-bias ultraviolet photodetector based on p-GaN/n-ZnO heterojunction
Applied Physics Letters **105**, 072106 (2014); 10.1063/1.4893591

Double side electroluminescence from p–NiO/n–ZnO nanowire heterojunctions
Applied Physics Letters **95**, 131117 (2009); 10.1063/1.3232244

Self-powered p-NiO/n-ZnO heterojunction ultraviolet photodetectors fabricated on plastic substrates

Md Rezaul Hasan,[1,2,a] Ting Xie,[1,3,a] Sara C. Barron,[4] Guannan Liu,[1,3] Nhan V. Nguyen,[5] Abhishek Motayed,[1,6] Mulpuri V. Rao,[2] and Ratan Debnath[1,b]

[1]*Materials Science and Engineering Division, Material Measurement Laboratory, National Institute of Standards and Technology, Gaithersburg, Maryland 20899, USA*
[2]*Department of Electrical and Computer Engineering, George Mason University, 4400 University Drive, Fairfax, Virginia 22030, USA*
[3]*Department of Electrical and Computer Engineering, University of Maryland, College Park, Maryland 20742, USA*
[4]*Materials Measurement Science Division, Material Measurement Laboratory, National Institute of Standards and Technology, Gaithersburg, Maryland 20899, USA*
[5]*Semiconductor and Dimensional Metrology Division, Physical Measurement Laboratory, National Institute of Standards and Technology, Gaithersburg, Maryland 20899, USA*
[6]*Institute for Research in Electronics and Applied Physics, University of Maryland, College Park, Maryland 20742, USA*

(Received 18 August 2015; accepted 22 September 2015; published online 1 October 2015)

A self-powered ultraviolet (UV) photodetector (PD) based on p-NiO and n-ZnO was fabricated using low-temperature sputtering technique on indium doped tin oxide (ITO) coated plastic polyethylene terephthalate (PET) substrates. The *p-n* heterojunction showed very fast temporal photoresponse with excellent quantum efficiency of over 63% under UV illumination at an applied reverse bias of 1.2 V. The engineered ultrathin Ti/Au top metal contacts and UV transparent PET/ITO substrates allowed the PDs to be illuminated through either frontside or backside. Morphology, structural, chemical, and optical properties of sputtered NiO and ZnO films were also investigated. © *2015 Author(s). All article content, except where otherwise noted, is licensed under a Creative Commons Attribution 3.0 Unported License.* [http://dx.doi.org/10.1063/1.4932194]

Plastic electronics are of great interest now due to their light weight and shock resistance for use in portable and wearable device applications such as displays, sensor arrays, curved circuits, curved detector arrays, sensor skins, and other large-area electronics.[1–5] Self-powered ultraviolet (UV) photodetectors (PDs) have also attracted considerable attention in recent years for their ability to operate sustainably without external power for the optical communication, environmental monitoring, missile plume detection, and digital imaging applications.[5–11] The self-powered PDs that have been demonstrated rely on the photovoltaic (PV) effect produced by the built-in electric field of a junction.[5–10] Based on interface features, self-powered PDs can be categorized into two types: Schottky junctions and p-n junctions. In both structures, the photogenerated electrons and holes are separated by the build-in electric field and collected at cathode and anode, respectively.

As a representative II-VI group semiconductor, ZnO is intrinsically n-type with 3.3 eV direct bandgap, 60 mV exciton binding energy, and additionally high radiation and chemical resistance.[12,13] For the UV PD applications, junctions that are composed of ZnO have been investigated extensively due to the excellent electrical and optical properties of ZnO.[8–10,12,14] Despite the advantage of simple fabrication process as well as low stray capacitance, high internal gain of ZnO based Schottky and metal-semiconductor-metal PDs, p-n junction structure appears to be more promising due to its

[a]M. R. Hasan and T. Xie contributed equally to this work.
[b]Author to whom correspondence should be addressed. Electronic mail: ratan.debnath@nist.gov.

 ©Author(s) 2015

stability, low or zero bias currents, high impedance, lower applied filed, and faster response.[8,14,15] p-type ZnO is an obvious choice to make p-n homojunction with intrinsic n-type ZnO but p-type doping is very difficult. Among the variety of p-type materials that have been employed to form p-n junction with ZnO, p-NiO stands out due to its band alignment with ZnO and its alloys in UV PD applications.[15,17,18] Although excellent figures of merits have been achieved in NiO/ZnO PDs, most of the devices have been fabricated on rigid substrates using high processing temperature without any self-powered behavior[16,17] which can limit their application on plastic substrates. On the other hand, some devices have shown very slow temporal response[18] that may not be suitable for high-speed device applications.

The combination of excellent sensitivity, fast response, and self-sufficiency of an UV PD enables the operation of portable or wearable sensing or monitoring devices without external power supplies, as well as possible application in energy harvesting systems[11] and such features are lacking in UV PDs. In this paper, we demonstrate radio frequency (rf)-sputtered p-NiO/n-ZnO heterojunctions as self-powered UV PDs. The devices are fabricated on transparent, conducting, and indium-doped tin oxide (ITO) coated PET (polyethylene terephthalate) substrates and deposited at low temperature. Top metal contacts of the p-n heterojunctions are engineered to be UV transparent, allowing illumination of devices through both the PET/ITO and top metal contacts. Chemical, structural, and optical properties of NiO and ZnO thin films were characterized. The measured performance of the PDs shows self-powered properties driven by photovoltaic effect with very fast temporal response, as well as excellent external quantum efficiency (EQE), detectivity, and UV to visible rejection ratio.

The PDs have been fabricated on PET substrates using rf sputtering and the deposited thin films/devices have been characterized. Details can be found here in Ref. 19. Figure 1(a) shows the schematic of the device structure whereas Fig. 1(b) shows the optical image of the same, demonstrating its transparency and flexibility. High-resolution AFM images of sputtered NiO and ZnO thin films exhibit nanoscale-sized grains and smooth surface (Fig. 1(c)). The estimated granularities of the deposited NiO and ZnO films are 20 ± 6 nm and 50 ± 14 nm, respectively. The measured root mean square (rms) roughness of the films is 1.13 nm for NiO and 3.24 nm for ZnO. The small grain size and smooth surface of prepared NiO and ZnO films allow them to form abrupt p-n heterojunctions.

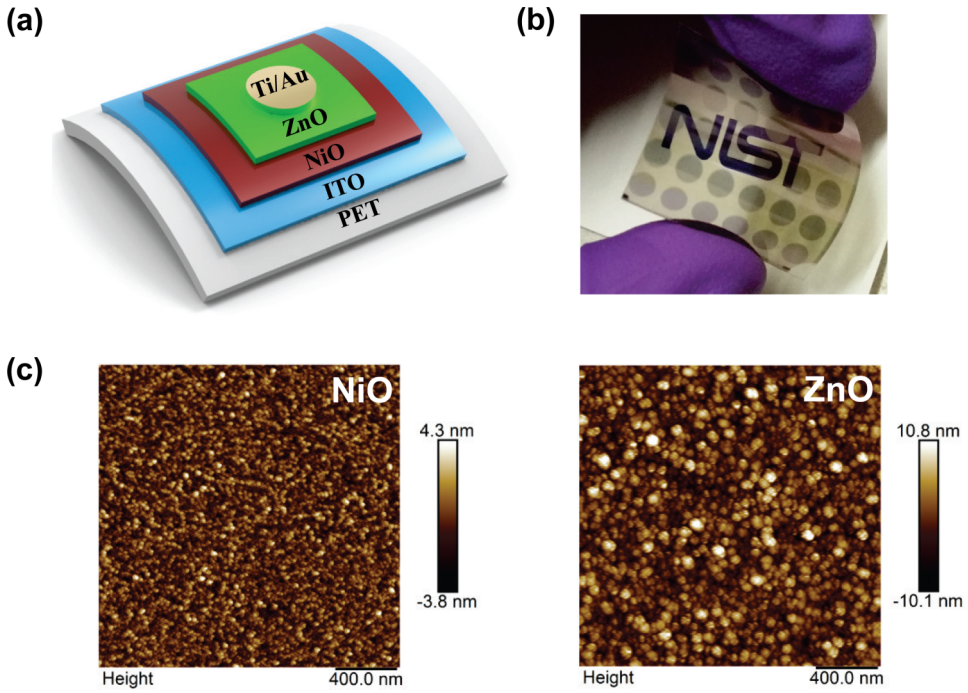

FIG. 1. (a) Schematic of the p-NiO/n-ZnO PD on PET/ITO substrate. (b) Actual optical image of the device exhibiting flexibility of the substrate. (c) AFM image of sputtered NiO and ZnO thin films. Nano-grains are clearly evident from AFM images.

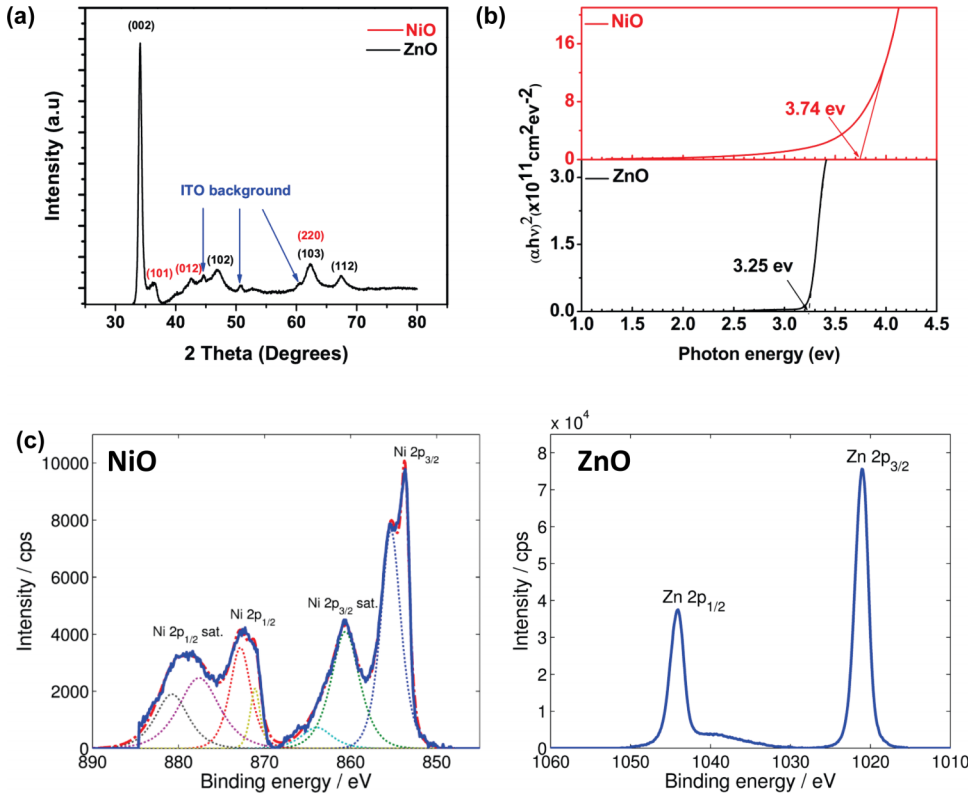

FIG. 2. (a) XRD scans taken from the fabricated device show diffraction peaks coming from different planes of NiO and ZnO. (b) Direct energy bandgap from absorption spectroscopy (Tauc plot). Both materials have direct energy bandgap. (c) XPS data for both NiO and ZnO films.

Grazing incidence X-ray diffraction (GIXRD) measurements of the fabricated device show all the diffraction peaks that can be assigned as cubic NiO (JCPDS-78-0643) or hexagonal wurtzite ZnO structure (JCPDS 36-1451), accordingly. GIXRD patterns of the individual films measured separately also indicate polycrystalline cubic NiO and hexagonal ZnO with broad diffraction peaks that are consistent with the small grain size.[19] The small grain sizes of the films agree well with the AFM results (Fig. 1(c)). Figure 2(b) shows the bandgaps of the NiO and ZnO thin films with Tauc plots measured by UV-vis spectroscopy. The bandgaps are estimated by extrapolating the linear region of the Tauc plots of $(\alpha h\nu)^2$ versus $h\nu$ to $h\nu = 0$, where α is the absorption coefficient and $h\nu$ is the photon energy. The estimated bandgaps are 3.74 eV and 3.25 eV for NiO and ZnO, respectively. The wide bandgaps lead to the transparency of the prepared films in the visible spectrum and will determine the rising and falling edges of the EQE patterns under various reverse bias voltages. High-resolution X-ray photoelectron spectroscopy (XPS) spectra of sputtered NiO and ZnO films at the Ni 2p and Zn 2p regions are shown in Fig. 2(c). Wide range low resolution scans (1 eV steps with a 160 eV pass energy) were used to check for contamination. In both NiO and ZnO films, the only elements identified were the desired metal oxide and carbon, attributed to surface contamination; neither Ni was found in the ZnO film nor Zn in NiO film (data not shown). As seen in spectrum of NiO, the Ni 2p 3/2 peak appears at a binding energy of 853.7 ± 0.1 eV, with the binding energy and multiplet splitting characteristics of Ni^{2+}, as in NiO.[20] In the spectrum of ZnO, the Zn 2p 3/2 peak at 1021.1 ± 0.1 eV, with 23.1 eV splitting from its 2p 1/2 component, is consistent with reported XPS data of other ZnO films.[21]

To illustrate the mechanism of the self-powered PDs, Fig. 3(a) shows the band diagrams of the fabricated device. Under UV illumination, electron-hole pairs are generated in the depletion region of the device. At the interface of NiO and ZnO films, the built-in electric field across the depletion region separates the photogenerated electron-hole pairs and drives them out of the depletion region. The

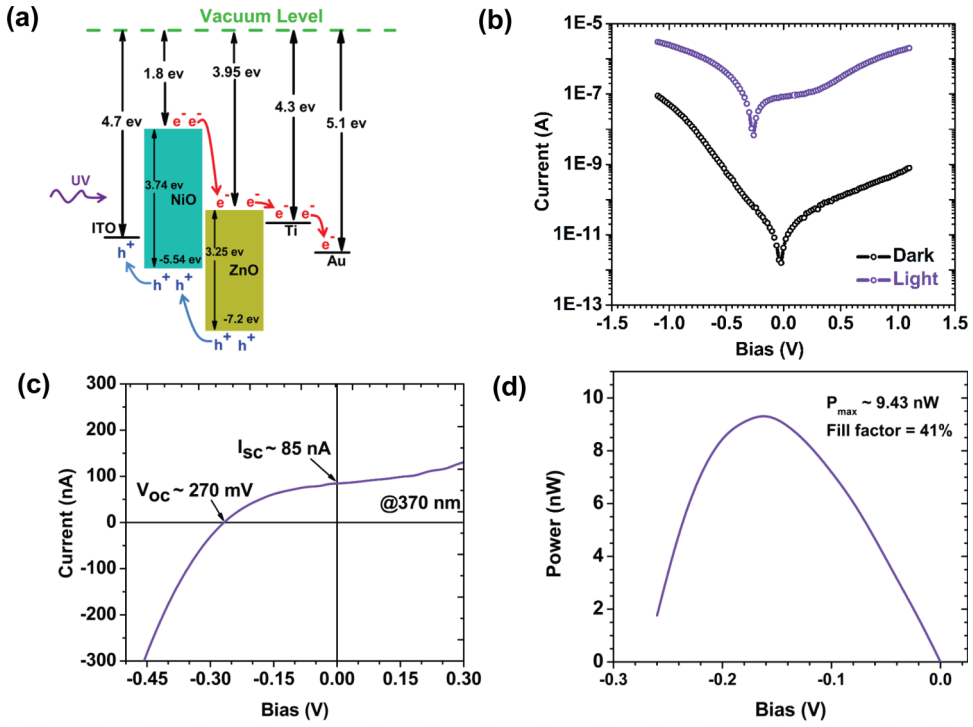

FIG. 3. (a) Energy levels of different components of PDs. Work function of all the components and bandgaps of NiO and ZnO films are shown. Under UV illumination, photogenerated holes and electrons in the depletion region of junction are collected by ITO side and metal contacts, respectively. (b) Diode characteristic of the device: I-V curve both in dark and under UV illumination at 370 nm. The device is illuminated through PET/ITO. The rectifying nature of the diode as well as the photoresponse is evident from the I-V data. The photoresponse factor, S, is found to be ~2700. (c) Self-powered behavior of the device showing open circuit voltage, $V_{oc} = 270$ mV and short circuit current, $I_{sc} = 85$ nA at 370 nm. Note that the typical beam size of the light source is smaller than the device area and the light intensity is ~12.1 μW. (d) Change of power in the voltage range of 0–V_{oc}.

drifted electrons then diffuse through the ZnO layer to be collected at the Ti/Au cathode. Similarly, the photogenerated holes reach to the ITO anode through the NiO layer.

Figure 3(b) shows the typical current-voltage (I-V) characteristics of p-NiO/n-ZnO heterojunction device in the dark and under UV illumination from the backside (PET/ITO) at room temperature. The applied voltage ranges from −1.2 V to 1.2 V, where the positive voltage means reversed bias. The diode shows an obvious rectifying behavior and a rectification ratio of ≈111 at ±1.2 V is calculated from the dark current. The obtained ideality factor n = 3.96 is greater than its normal range ($1 < n < 2$).[19] It implies that the transport mechanism is not dominated by the thermionic emission and it can be inferred that defects exist in the quasi-neutral region as well as in the junction which can be responsible for the carrier recombination at the junction.

The PV properties of the device under monochromatic UV excitation of 370 nm are also evident as shown in Fig. 3(c). The self-powered behavior can be attributed to the proper built-in electric field between NiO and ZnO arising from the perfect band-alignment (Fig. 3(a)). The open-circuit voltage (V_{oc}) which is the maximum voltage available from a PV cell at zero current and short-circuit current (I_{sc}) which is the current when the voltage across the cell is zero are measured to be 270 mV and 85 nA, respectively. As mentioned earlier, ideality factor of the diode is greater than one; hence, carrier recombination plays a major role and reduces V_{oc} significantly despite the large built-in-potential between NiO and ZnO. The PV effects make the fabricated devices suitable for self-powered PD application with monochromatic power conversion efficiency of 0.08% which can be further improved by engineering the materials. Figure 3(d) shows the calculated self-generated power with the forward bias in the range of 0–V_{oc} (270 mV). The maximum power point of curve is found at a voltage of $V_m = 0.16$ V and current $I_m = 50.8$ nA, yielding a maximum output power of 9.43 nW. The fill factor which is ratio of $V_m I_m / V_{oc} I_{sc}$ has been calculated to be ~41% for the device.

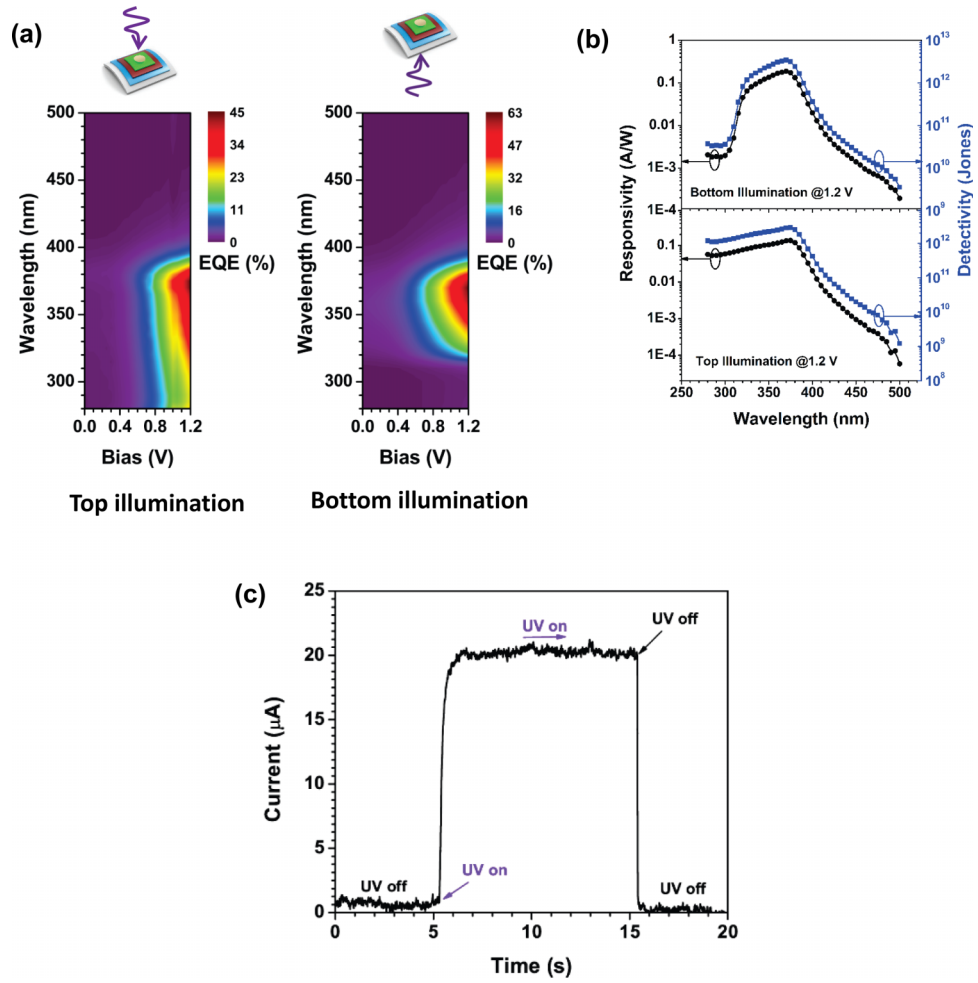

FIG. 4. Device performance: (a) measured EQE of the PD as a function of applied reverse bias with light illumination through the Ti/Au contact (top illumination-image to the left) and PET/ITO (bottom illumination-image to the right). The maximum EQE reaches to 45% for the former and 63% for the latter at 370 nm under 1.2 V reverse bias, and (b) calculated responsivity (left-axis) and detectivity (right-axis) of the same. (c) Time-resolved photocurrent response to a 10 s light pulse from 365 nm UV light source at 1.2 V reverse bias. Dark currents have been subtracted. The device has been illuminated through PET/ITO side.

Performances of NiO/ZnO devices have been measured at an applied reverse bias from 0 V to 1.2 V under top illumination (i.e., through Ti/Au metal contacts) as shown in Fig. 4(a). The light spectrum spans from 280 nm to 500 nm. The obtained device spectral response is normalized to the measured photocurrent of a NIST-calibrated Si photodetector under the identical illumination condition. At an applied reverse bias of 1.2 V, the maximum EQE reaches to ≈45% at 370 nm wavelength (image to the left of Fig. 4(a)). Detectivity (D^*) is another important specification that characterizes the capability of PDs to detect the weakest light signal. By regarding the dark current as the major component of the noise, the specific detectivity is defined by the expression

$$D^* = \frac{R_\lambda}{\sqrt{2eJ_{dark}}},$$

where e is the electron charge, R_λ is the responsivity at wavelength λ, and J_{dark} is the measured dark current at the same reverse bias of the used responsivity.[22] The responsivity (R_λ), the ratio of detected photocurrent to incident light intensity, shows the maximum value of ≈0.14 A/W at 370 nm at a reverse bias of 1.2 V (Fig. 4(b)). The calculated detectivity of the fabricated device at 370 nm reaches to a maximum of 2.9×10^{12} cm $\sqrt{\text{Hz}}$/W or Jones.

EQE of the PD is also measured while illuminating through the PET/ITO side (i.e., bottom illumination). At the reverse bias of 1.2 V, the EQE reaches ≈63% at 370 nm (image to the right of Fig. 4(a)). The calculated maxima D* and R_λ are found to be 3.8×10^{12} cm $\sqrt{\text{Hz}}$/W and ≈0.19 A/W, respectively (Fig. 4(b)). The distinct but higher performance of the PD under bottom illumination as compared to the top illumination is likely due to the higher transparency of the PET/ITO as compared to ultrathin Ti/Au electrode around the UV regime of 370 nm.[19] Additionally, the device shows a sharp cut-off wavelength at 320 nm under bottom illumination condition, which is due to the precipitous drop in the UV transparency profile of the PET/ITO around 320 nm. On the contrary, the device shows some performance under top illumination even at 280 nm, albeit lower, due to the some UV transparency of ultrathin Ti/Au at that wavelength or lower. These explain why the devices have distinct EQE pattern at lower wavelength although they look quite similar at higher wavelength. It must be mentioned here that no masking has been used for top illumination; hence, it is possible that carriers can be collected from the edges of contacts thus increasing EQE at lower wavelength despite very low transmission through the metals. Also, thickness uncertainty in ultrathin metal can dramatically change the transmission curve in Fig. S4[19] and influence the photoresponse.

Fig. 4(c) shows the temporal response of the fabricated photodetectors under 365 nm UV illumination at room temperature. The photocurrent increases very rapidly upon exposure to UV radiation, stays essentially constant during the UV exposure, and decays much faster when UV is turned off. The rise time (t_r) for the photocurrent to reach from 10% to 90% of its maximum value is ≈323 ms and the decay time (t_d) for the photocurrent to decrease from 90% to 10% of the peak value is ≈12 ms. The slow response of the PD is related to strong carrier trapping and these photoconductors exhibit comparable or better temporal response than other oxide based PDs[16,18] indicating high quality engineered metal oxide heterojunction with excellent sensitivity. The devices also demonstrate an excellent UV-selective sensitivity with maximum UV-to-visible rejection ratio ($R_{\lambda=370\text{nm}}/R_{\lambda=450\text{nm}}$) of ≈183.[19]

In this work, we have demonstrated self-powered photodiodes based on low-temperature rf-sputtered NiO and ZnO on PET/ITO substrates. The architecture of the device and the UV transparency of the substrate allow the illumination through both the top Ti/Au metal and bottom PET/ITO contacts side without significantly affecting the device performance. The fabricated *p*-NiO/*n*-ZnO heterojunction exhibits excellent UV sensitivity with a reasonable on/off ratio as well as self-powered behavior with V_{oc} of 270 mV, I_{sc} of 85 nA, and fill factor of ~41%. The maximum EQE of 63%, detectivity of 3.8×10^{12} cm $\sqrt{\text{Hz}}$/W, and responsivity of 0.19 A/W are achieved at 370 nm under a reverse bias of 1.2 V while illumination through the bottom side. Considering the advantages of low-temperature processable fabrication with large visible-blind UV selectivity detection as well as very fast temporal response, these heterojunction PDs have potential for use in large-area UV PD applications.

One of the authors (M.R.H.) acknowledges the financial support of NSF Grant No. 203146. The devices were fabricated in the Nanofab of the NIST Center for Nanoscale Science and Technology (CNST). The authors are grateful to Dr. Kerry Siebein and Dr. David J. Gundlach of NIST for their valuable help with XRD and EQE measurements, respectively.

[1] T. Someya, Nat. Mater. **9**(11), 879–880 (2010).
[2] J. Wang, C. Yan, M.-F. Lin, K. Tsukagoshi, and P. S. Lee, J. Mater. Chem. C **3**(3), 596–600 (2015).
[3] G. Chen, B. Liang, Z. Liu, G. Yu, X. Xie, T. Luo, Z. Xie, D. Chen, M.-Q. Zhu, and G. Shen, J. Mater. Chem. C **2**(7), 1270–1277 (2014).
[4] X. Xie and G. Shen, Nanoscale **7**(11), 5046–5052 (2015).
[5] Z. Gao, W. Jin, Y. Zhou, Y. Dai, B. Yu, C. Liu, W. Xu, Y. Li, H. Peng, Z. Liu, and L. Dai, Nanoscale **5**(12), 5576–5581 (2013).
[6] J. Qi, X. Hu, Z. Wang, X. Li, W. Liu, and Y. Zhang, Nanoscale **6**(11), 6025–6029 (2014).
[7] H.-Y. Chen, K.-W. Liu, X. Chen, Z.-Z. Zhang, M.-M. Fan, M.-M. Jiang, X.-H. Xie, H.-F. Zhao, and D.-Z. Shen, J. Mater. Chem. C **2**(45), 9689–9694 (2014).
[8] H. Zhou, P. Gui, Q. Yu, J. Mei, H. Wang, and G. Fang, J. Mater. Chem. C **3**(5), 990–994 (2015).
[9] Y. Shen, X. Yan, Z. Bai, X. Zheng, Y. Sun, Y. Liu, P. Lin, X. Chen, and Y. Zhang, RSC Adv. **5**(8), 5976–5981 (2015).
[10] Y. Q. Bie, Z. M. Liao, H. Z. Zhang, G. R. Li, Y. Ye, Y. B. Zhou, J. Xu, Z. X. Qin, L. Dai, and D. P. Yu, Adv. Mater. **23**(5), 649–653 (2011).
[11] S. Xu, Y. Qin, C. Xu, Y. Wei, R. Yang, and Z. L. Wang, Nat. Nanotechnol. **5**(5), 366–373 (2010).
[12] F. D. Auret, S. A. Goodman, M. Hayes, M. J. Legodi, H. A. van Laarhoven, and D. C. Look, Appl. Phys. Lett. **79**(19), 3074–3076 (2001).

[13] S. Das, S. Chakrabarti, and S. Chaudhuri, J. Phys. D: Appl. Phys. **38**(22), 4021–4026 (2005).
[14] S. M. Hatch, J. Briscoe, and S. Dunn, Adv. Mater. **25**(6), 867–871 (2013).
[15] T. Xie, G. Liu, B. Wen, J. Y. Ha, N. V. Nguyen, A. Motayed, and R. Debnath, ACS Appl. Mater. Interfaces **7**(18), 9660–9667 (2015).
[16] D. Y. Kim, J. Ryu, J. Manders, J. Lee, and F. So, ACS Appl. Mater. Interfaces **6**(3), 1370–1374 (2014).
[17] R. Debnath, T. Xie, B. M. Wen, W. Li, J. Y. Ha, N. F. Sullivan, N. V. Nguyen, and A. Motayed, RSC Adv. **5**(19), 14646–14652 (2015).
[18] Y. Vygranenko, K. Wang, and A. Nathan, Appl. Phys. Lett. **89**(17), 172105 (2006).
[19] See supplementary material at http://dx.doi.org/10.1063/1.4932194 for thin film deposition and characterization.
[20] M. C. Biesinger, B. P. Payne, L. W. M. Lau, A. Gerson, and R. S. C. Smart, Surf. Interface Anal. **41**(4), 324–332 (2009).
[21] X. Liu, J. Zhang, L. Wang, T. Yang, X. Guo, S. Wu, and S. Wang, J. Mater. Chem. **21**(2), 349–356 (2011).
[22] N. Park, K. Sun, Z. Sun, Y. Jing, and D. Wang, J. Mater. Chem. C **1**(44), 7333–7338 (2013).